Electronic Supplementary Material (ESI) for Journal of Materials Chemistry A.

Construction of $NiCo_2O_4$@graphene Nanorods by Tuning the Compositional Chemistry of Metal Organic Frameworks with Enhanced Lithium Storage Properties

Zhiqing Jia,[a,b] Yingbin Tan,*[a] Zhonghui Cui,[a] Linlin Zhang [a] and Xiangxin Guo *[ac]

[a] *State Key Laboratory of High Performance Ceramics and Superfine Microstructure, Shanghai Institute of Ceramics, Chinese Academy of Sciences, Shanghai 200050, China. *Email: tanyingbin1986@126.com; xxguo@mail.sic.ac.cn*
[b] *University of Chinese Academy of Sciences, Beijing 100039, China. of Sciences, Beijing 100039, China.*
[c] *College of Physics, Qingdao University, Qingdao 266071, China.*

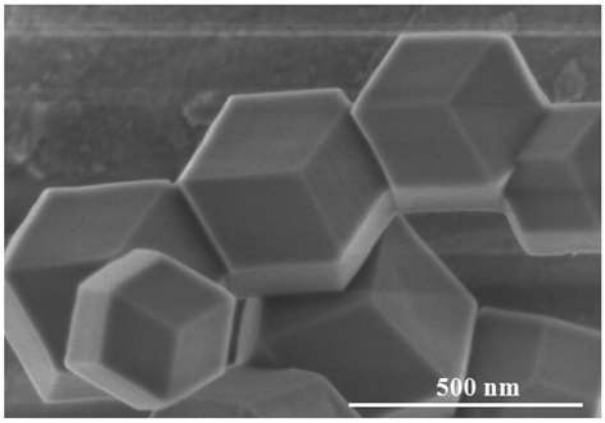

Fig. S1 SEM image of ZIF-67 precursor.

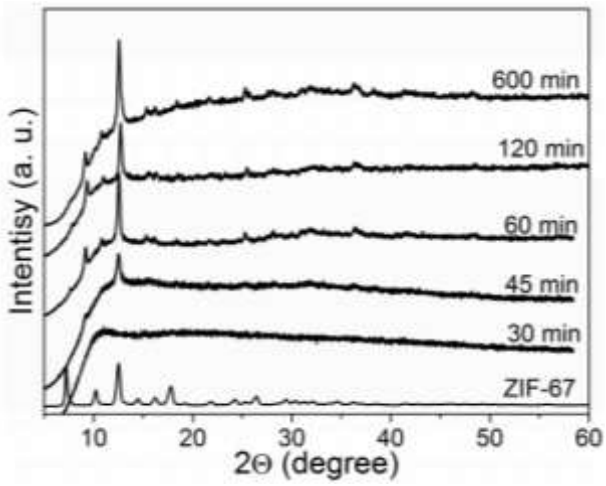

Fig. S2 XRD patterns of ZIF-67@Ni-BTC obtained with reaction time of 30 min, 45min, 60 min, 120 min and 600 min.

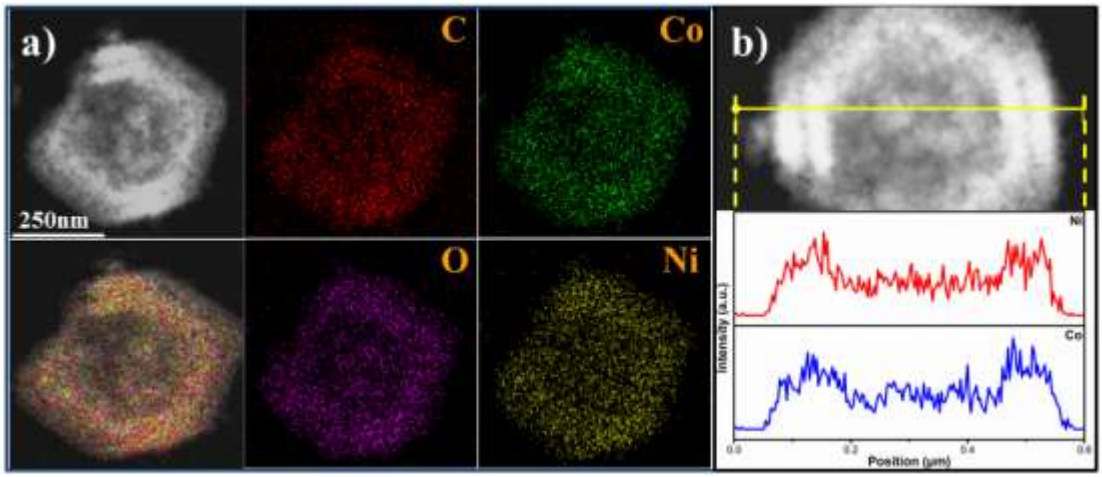

Fig. S3 a) STEM and Elemental mapping images and b) Line profiling analysis of the ZIF-67@Ni-BTC with reaction time of 10 min.

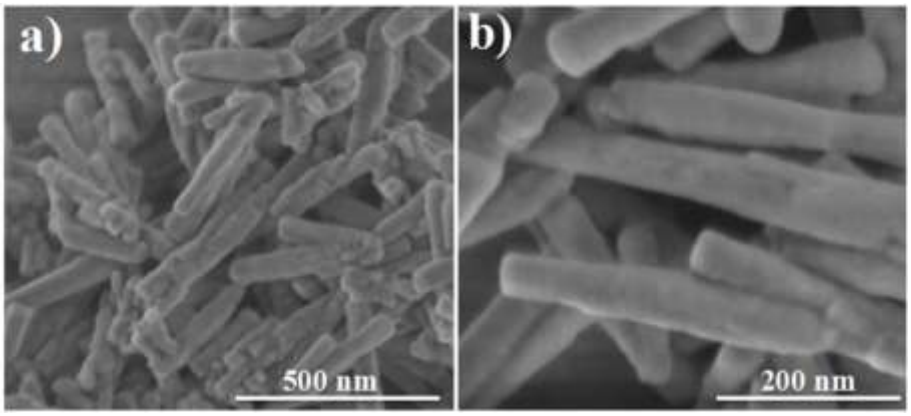

Fig. S4 SEM images of ZIF-67@Ni-BTC nanorods.

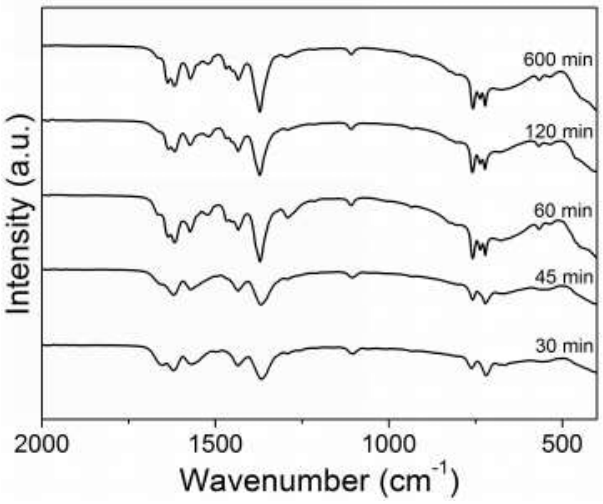

Fig. S5 FTIR patterns of ZIF-67@Ni-BTC obtained with reaction time of 30 min, 45min, 60 min, 120 min and 600 min.

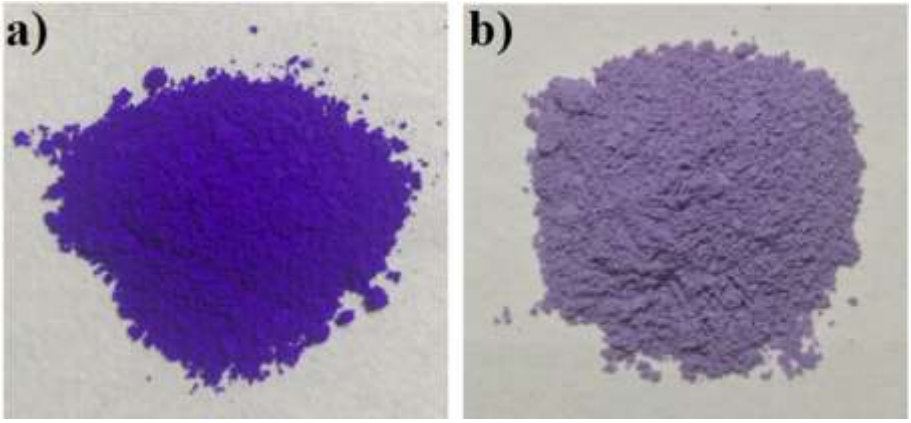

Fig. S6 The photos of a) ZIF-67 and b) ZIF-67@Ni-BTC nanorods.

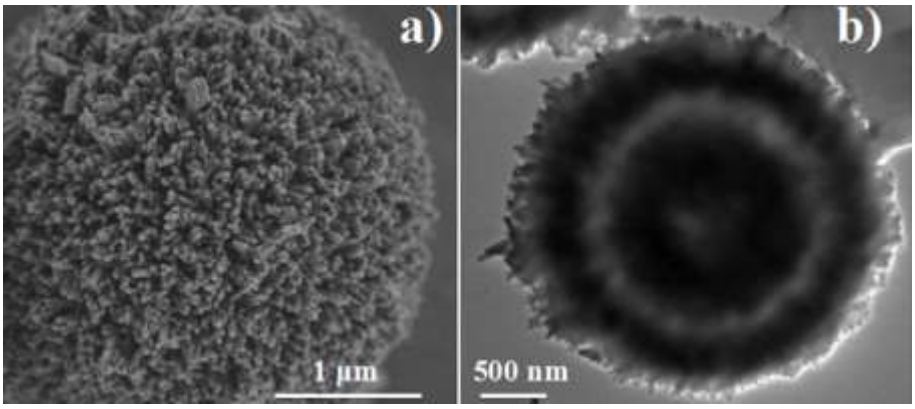

Fig. S7 a) SEM and b) TEM images of NiCo-BTC.

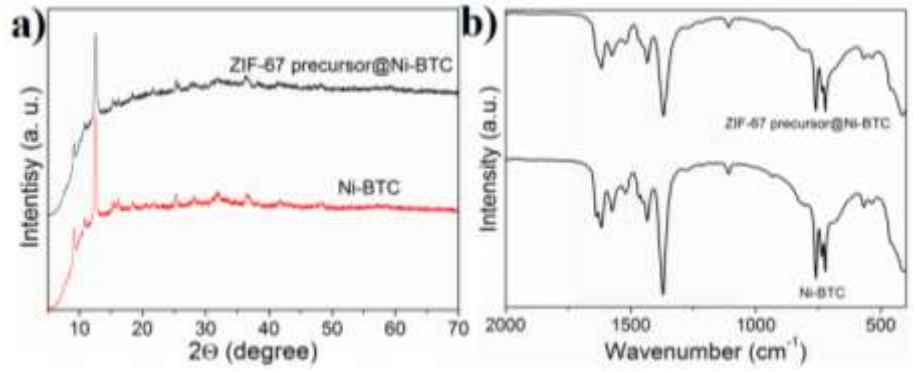

Fig. S8 a) XRD and b) FTIR patterns of ZIF-67@Ni-BTC nanorods and Ni-BTC.

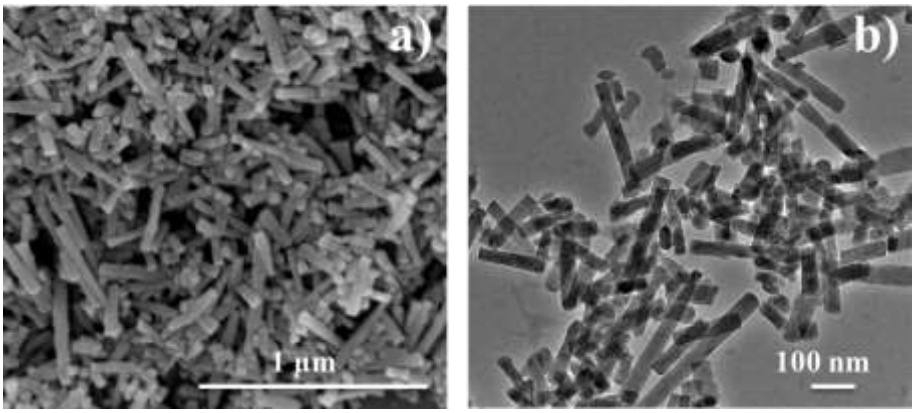

Fig. S9 a) SEM and b) TEM images of ZIF-67@Ni-BTC nanorods with the presence of ZIF-67's precursors (cobalt nitrate and 2-methylimidazole) and nickle nitrate and BTC.

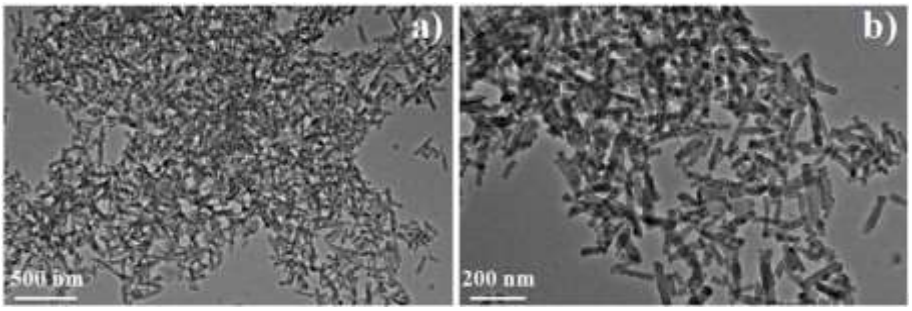

Fig. S10 TEM images of ZIF-67@NiCo-BTC.

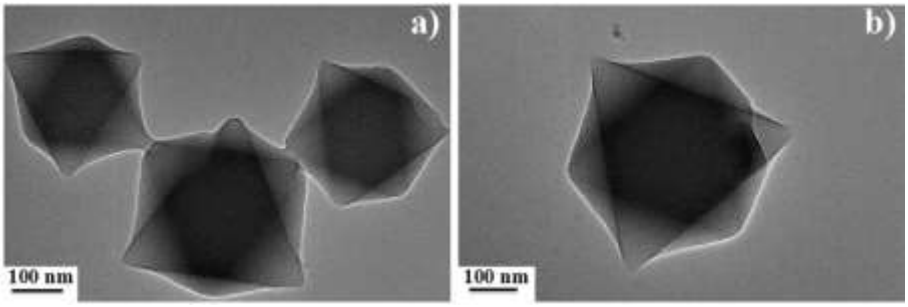

Fig. S11 TEM images of ZIF-67@Cu-BTC.

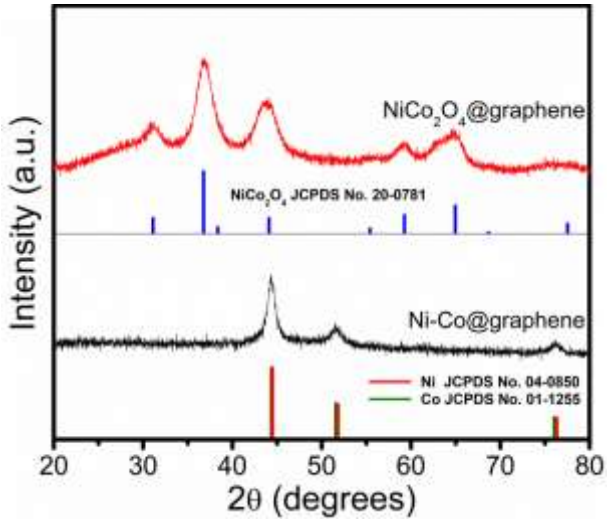

Fig. S12 XRD patterns of Ni-Co@graphene and $NiCo_2O_4$@graphene nanorods.

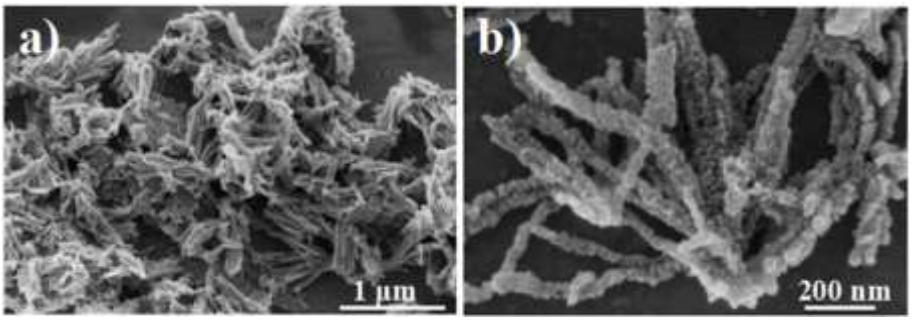

Fig. S13 SEM images of Ni-Co@graphene.

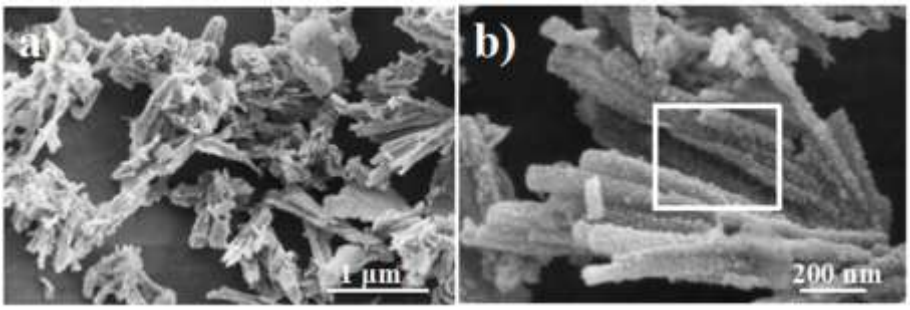

Fig. S14 SEM images of $NiCo_2O_4$@graphene nanorods.

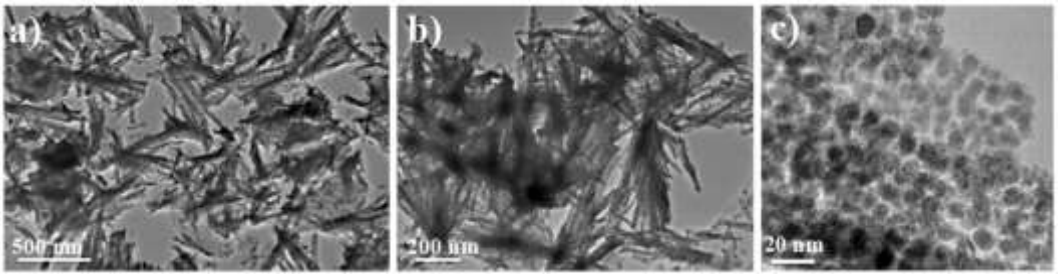

Fig. S15 a), b) TEM images and c) HRTEM image of $NiCo_2O_4$@graphene nanorods.

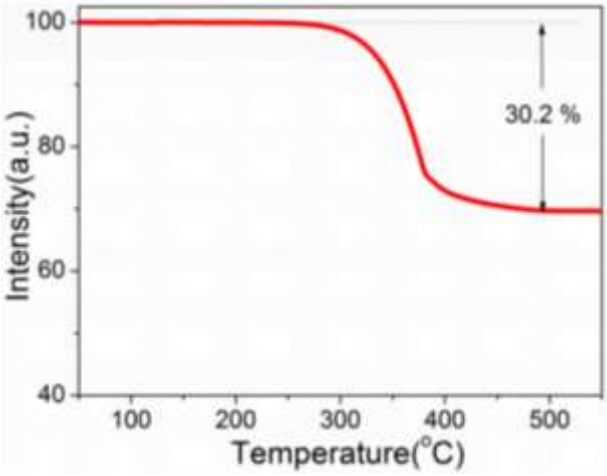

Fig. S16 TGA curve of $NiCo_2O_4$@graphene nanorods.

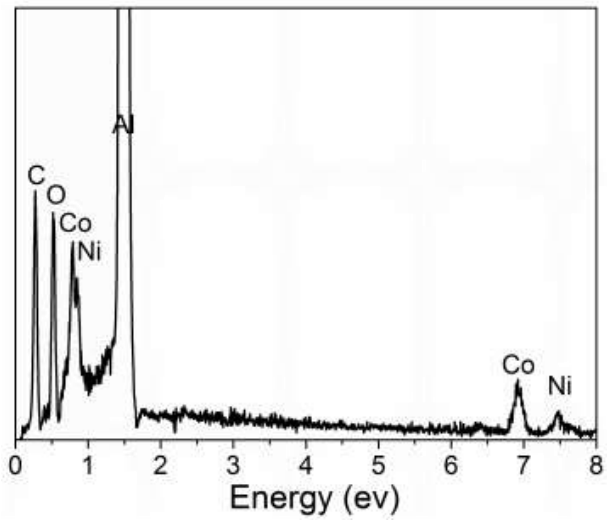

Fig. S17 EDX spectrum of the area in the white square of Fig. S13b.

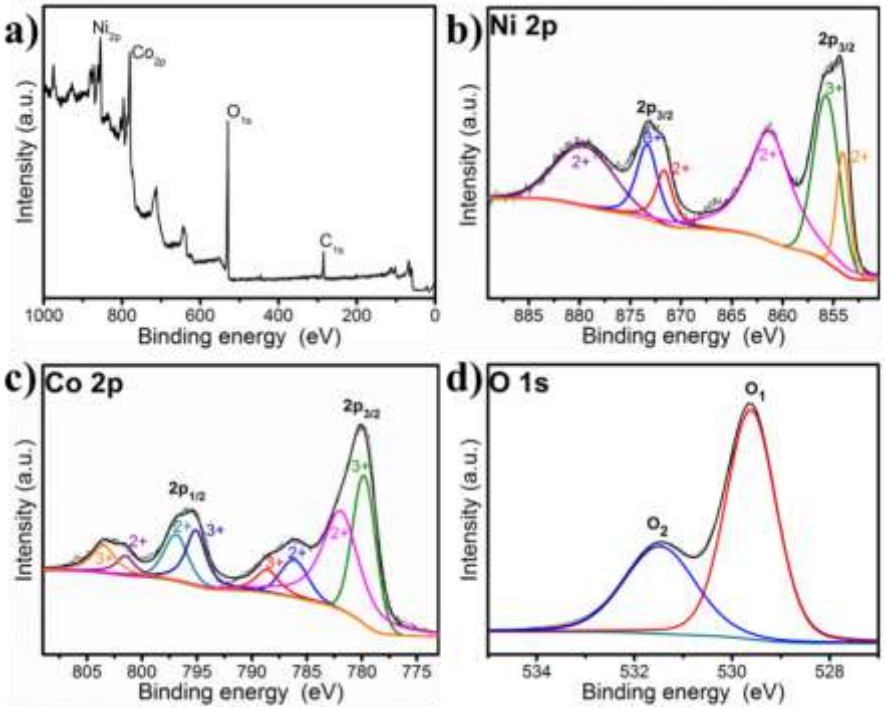

Fig. S18 a) Survey XPS spectrum and high-resolution XPS spectrum for the b) Ni 2p, c) Co 2p and d) O 1s region of the $NiCo_2O_4$@graphene nanorods.

The Ni 2p spectra (Fig. S18b) confirms the presence of Ni^{2+} and Ni^{3+}, the peaks at 854.2 and 871.9 eV are indexed to Ni^{2+}, while other peaks at 855.6 and 873.6 eV are associated with Ni^{3+}. Likewise, Co 2p spectra reveals two types of Co species can be observed in the Fig. S17c. The peaks at 780.5 and 796.0 eV are assigned to Co^{2+}, while other peaks at 779.3 and 794.0 eV are belonged to Co^{3+}, which is in good accord with the previous results. The peaks

of O 1 (Fig. S18d) at 529.3 eV and O 2 at 530.8 eV are ascribed to the metal-oxygen and some adefect sites with low oxygen coordination. These results show that the chemical composition of $NiCo_2O_4$@graphene nanorods contain Ni^{2+}, Ni^{3+}, Co^{2+} and Co^{3+}, which are in good agreement with the results in the literature for $NiCo_2O_4$.

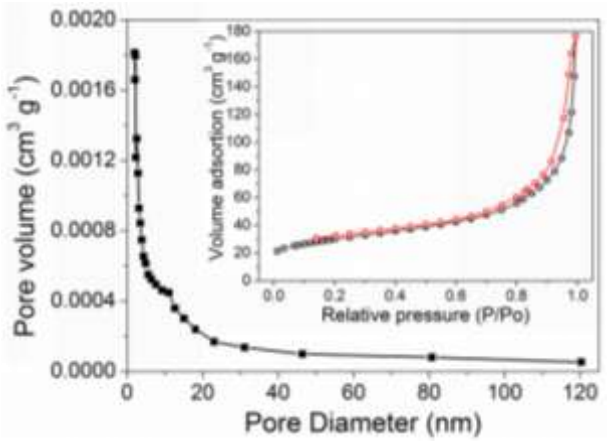

Fig. S19 Pore-size distribution and nitrogen adsorption-desorption isotherms (inset) of $NiCo_2O_4$@graphene nanorods.

The porosity of $NiCo_2O_4$@graphene nanorods could be verified by Brunauer-Emmett-Teller (BET) measurements. From the N_2 adsorption/desorption isotherm shown in the inset of Fig. S19, a reversible N_2 hysteresis loop in the range 0.8-1.0 p/p_0 was observed with typical type IV sorption behavior, suggesting the unique characteristic of a mesoporous microstructure of the $NiCo_2O_4$@graphene nanorods. Based on the that, the specific surface area and the pore volume of the $NiCo_2O_4$@graphene nanorods are calculated to be 105.3 m^2 g^{-1} and 0.26 cm^3 g^{-1}, respectively. Such a mesoporous $NiCo_2O_4$@graphene nanorods with the high surface areas and porous characteristics can facilitate the sufficient penetration of electrolyte and the fast transport of Li^+ as well as buffer the volume variation of $NiCo_2O_4$ nanoparticles, thus leading to high specific capacity and excellent cycling stability of the electrodes.

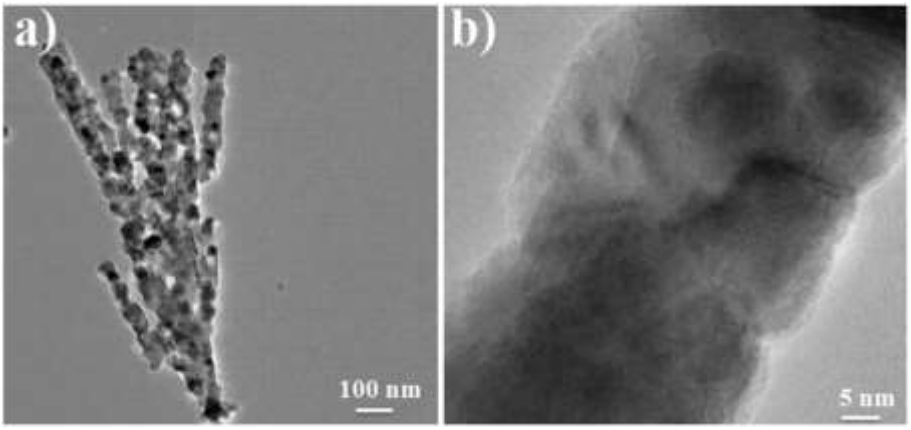

Fig. S20 a) TEM and b) HRTEM images of bare $NiCo_2O_4$ nanorods.

For comparison and demonstrating the internal distribution of $NiCo_2O_4$ phase in the porous $NiCo_2O_4$@graphene nanorods composites, the original ZIF-67@Ni-BTC nanorods were directly heating at 500 ^oC for 3 h in air to obtain the bare $NiCo_2O_4$ nanorods without carbon shells. After removing carbon matrix, the bare $NiCo_2O_4$ nanorods also inherited the general appearance of ZIF-67@Ni-BTC nanorods, and a large number of $NiCo_2O_4$ nanoparticles stacked into a 1D porous $NiCo_2O_4$ nanostructure.

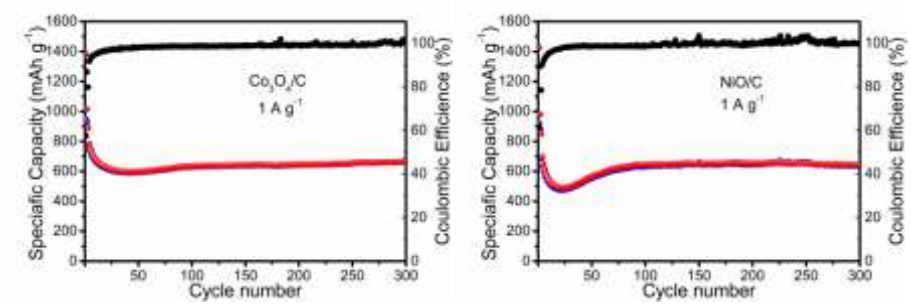

Fig. S21 The cycling performance and Coulombic efficiencies of Co_3O_4/C and NiO/C at 1 A g^{-1}.

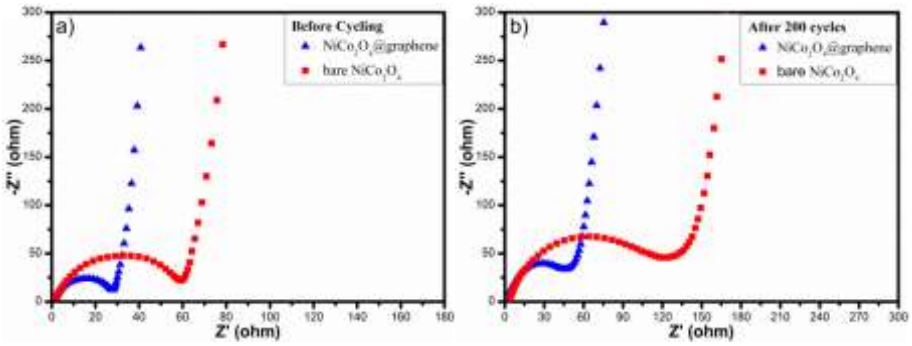

Fig. S22 Nyquist plots of the $NiCo_2O_4$@graphene and bare $NiCo_2O_4$ a) before cycling and b) after the 200th cycle with a fully charged state.

Electrochemical impedance spectroscopy (EIS) measurements of the two electrodes were carried out to explain the superior electrochemical properties of the $NiCo_2O_4$@graphene composite compared with that of the bare $NiCo_2O_4$. The Nyquist plots obtained before and after 200 cycles are shown in Fig. S22. The resulting Nyquist plots all displayed a semicircle in the medium frequency region, which can be assigned to the charge-transfer resistance, followed by a slop line. Before cycling, the two electrodes show almost the same semicircle meaning similar charge-transfer resistances while with different increasing after cycling, as shown in Fig. S22a. For the $NiCo_2O_4$@graphene electrode, the slightly increased semicircle diameter (30 to 45 ohm) indicates its good stability during cycling. In contrast, the semicircle diameter for the bare $NiCo_2O_4$ electrode increased about one time after cycling, which mainly due to the cycling-induced structural degradation. This suggests that the graphene coating significantly facilitated the electron transfer and Li^+ ions diffusion and maintained the structure integrity during cycling.

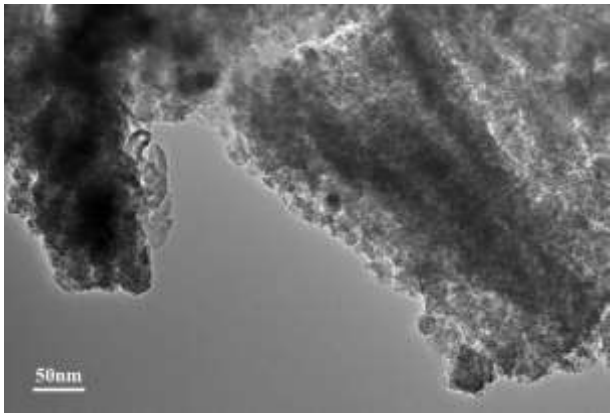

Fig. S23 TEM image of the $NiCo_2O_4$@graphene electrode after 1200 cycles at 500 mA g^{-1}.

Table S1 The ratio of C, O, Ni and Co in the NiCo2O4@graphene nanorods based on the XPS result.

Sample	C (wt%)	O (wt%)	Co (wt%)	Ni (wt%)

$NiCo_2O_4$/graphene	30.3	23.8	30.5	15.4

Table S2 Electrochemical performance of different $NiCo_2O_4$-based electrodes

Type of $NiCo_2O_4$	Initial discharge capacity (mAh g^{-1})	Rate performance (mAh g^{-1})	Capacity retention after cycling	Reference
$NiCo_2O_4$-RGO	1351 at 100 mA g^{-1}	396 at 0.8 A g^{-1}	~65% after 110 cycles at 200 mA g^{-1}	S1
$NiCo_2O_4$@ Au NTs	1310 at 100 mA g^{-1}	349 at 5 A g^{-1}	~69% after 200 cycles at 100 mA g^{-1}	S2
$NiCo_2O_4$ nanoflakes	1292 at 500 mA g^{-1}	~780 at 2 A g^{-1}	~62.5% after 100 cycles at 800 mA g^{-1}	S3
$NiCo_2O_4$ NWAs	1291 at 100 mA g^{-1}	810 at 1 A g^{-1}	~72% after 50 cycles at 500 mA g^{-1}	S4
$NiCo_2O_4$ mesoporous microspheres	1680 at 100 mA g^{-1}	393 at 1.6 A g^{-1}	~58.7% after 500 cycles at 800 mA g^{-1}	S5
flower-like $NiCo_2O_4$	1280 at 150 mA g^{-1}	~420 at 2 A g^{-1}	~55% after 60 cycles at 500 mA g^{-1}	S6
$NiCo_2O_4$@ graphene nanorods	**1303 at 500 mA g^{-1}**	**505 at 4 A g^{-1}**	**83.5% after 1200 cycles at 1000 mA g^{-1}**	**This work**

S1. Y. Chen, M. Zhuo, J. Deng, Z. Xu, Q. Li and T. Wang, *J. Mater. Chem. A*, 2014, **2,** 4449-4456.

S2. J. Zhu, Z. Xun and B. Lu, *Nano Energy*, 2014, **7,** 114-123.

S3. A. K. Mondal, D. Su, S. Chen, X. Xie and G. Wang, *ACS Appl. Mater. Interfaces*, 2014, **6,** 14827-14835.

S4. X. Zhou, G. Chen, J. Tang, Y. Ren and J. Yang, *J. Power Sources*, 2015, **229,** 97-103.

S5. J. Li, S. Xiong, Y. Liu, Z. Ju and Y. Qian, *ACS Appl. Mater. Interfaces*, 2013, **5,** 981-988.

S6. L. Li, Y. Cheah, Y. Ko, P. Teh, G. Wee, C. Wong, S. Peng and M. Srinivasan, *J. Mater. Chem. A*, 2013, **1,** 10935-10941.